Synthesis and thermal conductivity of functionalized biocarbon-Fe_3O_4 nanocomposite-based green nanofluid for heat transfer applications

Divya Barai, *Sohan* Parbat, and *Bharat* Bhanvase*

Department of Chemical Engineering, Laxminarayan Institute of Technology, Rashtrasant Tukadoji Maharaj Nagpur University, Nagpur 440033, MS, India

Abstract. Bio-based graphitic carbon was synthesized in this work by one-step carbonization of bamboo waste at low temperature. This bio-based carbon was then functionalized in order to decorated it with Fe_3O_4 nanoparticles. The functionalized biocarbon-Fe_3O_4 (f-biocarbon-Fe_3O_4) nanocomposite was synthesized using ultrasound-assisted coprecipitation method which was then confirmed by scanning electron microscopy, Fourier transform infrared spectroscopy, and X-ray diffractometry. Water-based nanofluid was prepared using the synthesized f-biocarbon-Fe_3O_4 nanocomposite particles. Thermal conductivity of this nanofluid was analyzed at different concentrations and temperatures. A thermal conductivity enhancement of almost 80% was recorded at 35°C for nanofluid containing 0.1 vol.% of f-biocarbon-Fe_3O_4 nanocomposite particles compared to water. Also, empirical model is developed for prediction of thermal conductivity as a function of concentration and temperature of bamboo waste-derived f-biocarbon-Fe_3O_4 nanocomposite-based green nanofluid.

* Corresponding author: bharatbhanvase@gmail.com

1 Introduction

Nanofluids have gained much importance ever since their superior thermal properties are realized. Several investigations are carried out to reveal their performance in various heat transfer processes including those in automobile radiator, refrigeration, electronic cooling devices, solar thermal collectors etc. These applications are therefore known to be benefited by the use of nanofluids as far as energy conservation is concerned [1–3]. For the same, different nanomaterials have been synthesized and analysed. Mostly, metal and metal oxides, which are known to possess high thermal conductivity, have been applied as candidates for nanofluid synthesis [4–8]. However, nanoparticles of metals and metal oxides have a tendency to agglomerate which is not desired for nanofluid applications as it leads to deterioration of nanofluid thermal conductivity [9,10]. Simultaneously, carbon-based materials, especially graphene and carbon nanotubes have also gained immense attention in energy field due to their superior thermal and electrical properties [11–15]. This has led to their use in synthesizing nanofluids for heat transfer as well [16–18]. The technological advancement has made provision for synthesis of nanocomposite materials (composed of two or more materials of which at least one is nanosized). In view of this, many nanocomposite particles have been synthesized and tested for nanofluid applications [19–28].

Many nanomaterials, often synthesized using harmful chemicals and energy-intensive processes, also possess many environmental hazards, which reduces their attractiveness as far as sustainable development is concerned. With the rise in awareness for environmentally friendly materials, different types of bio-derived nanostructures are being prepared by using easily available, low-cost and eco-friendly waste materials. This not only contributes as a value-addition but also in reducing waste. Mostly, carbon nanostructures have been widely synthesized using bio-waste material [29]. Biobased materials have potential to replace fossil fuels for production of porous carbon for numerous applications [30]. Conversion processes mainly involve pyrolyzing the biobased materials at high temperature thereby generating different gaseous or liquid fuels and carbon, commonly known as biochar. Application of bio-derived carbon nanostructures in supercapacitors batteries, wastewater treatment, electrochemical sensing devices, dye sensitised solar cells and as catalysts etc. have already been identified [31–35].

Different biobased materials are innovatively converted to nanomaterials for different nanofluid applications. Esmaeilzadeh et al. [36] synthesized nanofluids for pharmaceutical and food applications using whey protein nanospheres. The various methods developed could yield nanofluids that could stay stable upto an year. Abraham et al. [37] synthesized ZnO nanoparticles and studied their surface modification via bio-capping using *Scorparia dulcis* which is a medicinal plant. It was found that the surface modified-ZnO nanoparticles could significantly enhance thermal conductivity of ethylene glycol and water by 14.68% and 11.41%, respectively at nanoparticle weight percentage of 0.005. Okonkwo et al. [38] used olive leaf extract (OLE) and barley husk (BH) for synthesis of TiO_2 and SiO_2 nanoparticles, respectively for application as nanofluid in parabolic trough collector. The OLE-TiO_2 and BH-SiO_2 nanoparticles based nanofluids exhibited an enhancement of 128% and 138%, respectively (compared to water) in the heat transfer coefficient which was attributed to improved thermal properties. Further, synthesis of covalent functionalization graphene nanoplatelets (CGNPs) was carried out using clove buds so as to increase stability of graphene nanoplatelets (GNPs) in polar solvents [39]. In this, eugenyl acetate, eugenol, and β-caryophyllene from the cloves was grafted over the surface of GNPs with the aid of hydrogen peroxide (free-radical oxidizer) and ascorbic acid (redox initiator). A 36.5% enhancement in convective heat transfer coefficient was observed for water-based nanofluids containing 0.1 wt.% CGNPs flowing in a straight stainless steel tube (1.4m in length) at Reynolds number of 15,925 which was a result of thinning of the thermal boundary layer due to enhanced thermal conductivity. All these studies only aimed to use biobased materials in the synthesis process either as modifying or as functionalizing agents. There was no direct conversion of the bio-based materials into carbon structures. The authors could find only one study reporting green nanofluid made out of carbon nanostructures derived from biobased materials wherein carbon nanospheres and nanotubes and were prepared using coconut fibre-activated carbon [40]. For this, the coconut fibre was carbonized and then activated by physical treatment. It was then treated using ethanol vapor at high temperatures (700°C to 1100°C). However, the investigation only reported density of the prepared ethylene glycol/water mixture-based nanofluids containing the synthesized carbon nanostructures and no data on thermal conductivity was informed.

As far as heat transfer application of green nanofluid is concerned, among all thermophysical properties, thermal conductivity is most important. Therefore, in this work, thermal conductivity of bamboo-derived green nanofluid has been investigated. This kind of study has been conducted for the first time.

2 Experimental

2.1 Materials

The bamboo waste used in this work was acquired locally from Nagpur, India. The chemicals used for synthesizing f-biocarbon-Fe_3O_4 nanocomposite particles from bamboo waste include $NaNO_3$, $KMnO_4$ (99%), $FeSO_4.7H_2O$ (99%), and NaOH purchased from Loba Chemie Pvt Ltd., India. H_2O_2 (30%), HCl (37%), and $FeCl_3$ (96%) were purchased from Merck Specialities Pvt Ltd., India. Also, H_2SO_4 (98%) was bought from S D Fine-Chem Limited, India and ethanol (99.9%) was

purchased from Changshu Hongsheng Fine Chemical Co. Ltd., India.

2.2 Synthesis of graphitic carbon

To synthesize bio-derived graphitic carbon, the bamboo waste (raw) was mixed with concentrated H_2SO_4 in the ratio 2:5 (weight by weight). This mixture was kept as it is for an hour for impregnation and was then shifted to a muffle furnace in a crucible. It was then heated at 160°C for 2 h for graphitization. After cooling, the obtained graphitic biocarbon powder was washed with water until neutral pH. It was oven-dried at 105°C for 2 h and was preserved for further processing.

2.3 Functionalization of the graphitic carbon

In order to functionalize the synthesized graphitic biocarbon by imparting oxygen functionalities to its surface, Hummers' method [41] was used. For this, 1 g of the synthesized biocarbon was used and the process similar to that used by Barai et al. [27] was adopted. The synthesized product was named as f-biocarbon.

2.4 Synthesis of f-biocarbon-Fe_3O_4 nanocomposite

For synthesis of f-biocarbon-Fe_3O_4 nanocomposite particles, 0.3 g of f-biocarbon was added to 50 ml distilled water and was sonicated for 5 min. Further, aqueous solutions (50 ml each) of $FeCl_3$ (0.04 M) and $FeSO_4.7H_2O$ (0.02 M) were added to the existing mixture. This mixture was further sonicated for 5 min. After this, NaOH solution (1 M) was added dropwise to this mixture till pH reached 11 in presence of ultrasonication while co-precipitation continued. This mixture was further sonicated for the next 20 min. After this, the formed f-biocarbon-Fe_3O_4 nanocomposite particles were filtered. They were then washed with distilled water and ethanol, and dried at 105°C in an oven for 2 hr.

2.5 Characterization

An electron micrograph image of the prepared f-biocarbon-Fe_3O_4 nanocomposite particles was obtained from a Scanning Electron Microscope (SEM) (JEOL JSM-6380). Fourier Transform Infrared (FTIR) spectroscopy of prepared nanoparticles was carried out using FTIR Spectrometer (Bruker Corporation, Alpha II). Also, an X-Ray diffractometer (Rigaku Miniflex 1800) was used to obtain the X-Ray diffraction (XRD) pattern of synthesized nanoparticles.

2.6 Preparation of f-biocarbon-Fe_3O_4 nanocomposite based nanofluid

Water-based nanofluids at various volume concentrations (0.025, 0.05, 0.075, and 0.1%) of f-biocarbon-Fe_3O_4 nanocomposite particles were prepared by ultrasonication.

2.7 Measurement of thermal conductivity of nanofluid

For measurement of thermal conductivity of f-biocarbon-Fe_3O_4 nanocomposite based nanofluid, the samples of nanofluid were initially ultrasonicated. Measurements were carried out using KD2 Pro Thermal Properties Analyzer (Decagon Devices, Inc., USA) with the aid of KS-1 sensor provided along with it. Thermal conductivity of nanofluid at different concentrations were measured at different temperatures (25°C to 45°C).

3 Results and discussion

3.1 Characterisation of f-biocarbon-Fe_3O_4 nanocomposite

SEM image of synthesized f-biocarbon-Fe_3O_4 nanocomposite particles is represented in Figure 1(a). Attachment of Fe_3O_4 nanoparticles after the process of ultrasound-assisted co-precipitation over the bamboo-based f-biocarbon structure can be clearly observed. Further, Figure 1(b) depicts a histogram of particle size of Fe_3O_4 nanoparticles attached to the f-biocarbon surface.

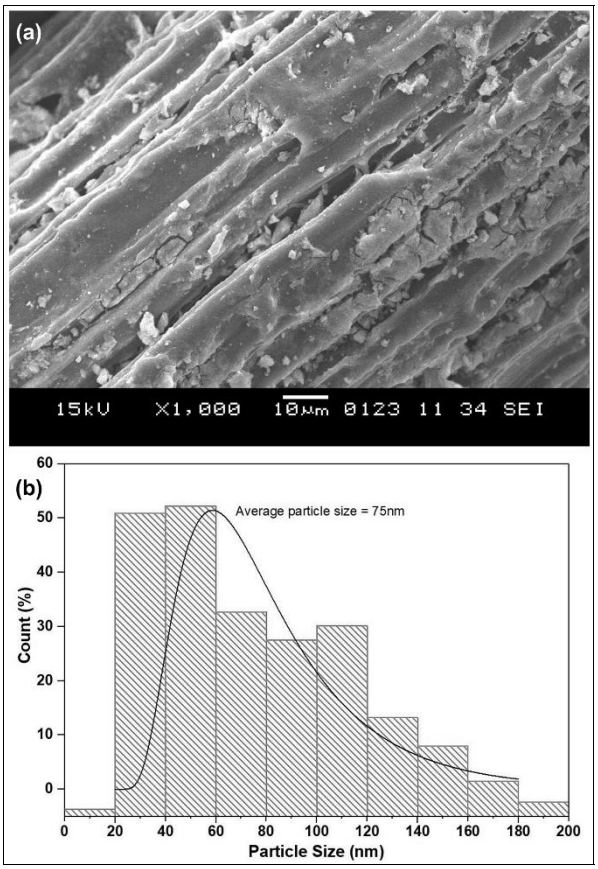

Fig. 1. (a) SEM image of f-biocarbon-Fe_3O_4 nanocomposite particles and (b) histogram of particle size of Fe_3O_4 nanoparticles

It has been found that the size distribution of the attached particles ranges from 20 to 200nm and the average size of the nanoparticles is 75nm. This small

size of the Fe_3O_4 nanoparticles covering the f-biocarbon surface is a result of ultrasonication which enabled efficient co-precipitation and prevented agglomeration of the nanoparticles. The cavities formed due to the high frequency ultrasound waves produce localised high temperature (10000 K) and pressure (1000 atm) conditions which aid in efficient nucleation and breaking down of the formed nanoparticles into smaller ones. The effective mixing action assists the nucleates to capture the oxygen functionalities present over the f-biocarbon surface. At the same time, this mixing action also helps to separate each f-biocarbon particle so as to expose its surface for attachment of the Fe_3O_4 nanoparticles. This has enabled uniform distribution of the Fe_3O_4 nanoparticles over the f-biocarbon particles. Still, some agglomeration is observed at some regions which can be because of the uneven surface of the f-biocarbon which may have concentrated oxygen functionalities locally thereby attracting a greater number of nucleates. There are also possibilities of most of the Fe_3O_4 nanoparticles to get trapped within the matrix of the carbon microstructure. However, maximum nanoparticles possess size of 40-60nm.

Figure 2 shows the FTIR spectra of raw bamboo waste, synthesized biocarbon, f-biocarbon and f-biocarbon-Fe_3O_4 nanocomposite.

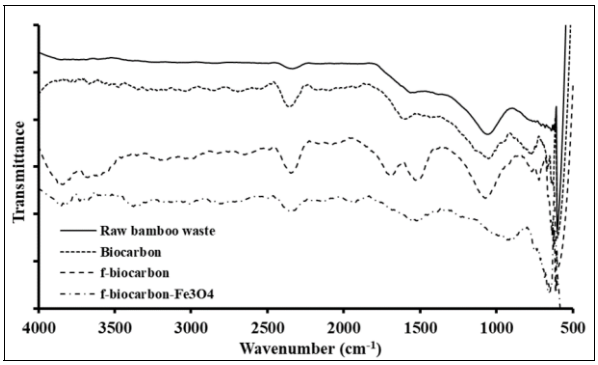

Fig. 2. FTIR spectra of raw bamboo waste, biocarbon, f-biocarbon and f-biocarbon-Fe_3O_4 nanocomposite particles

Presence of peak at 1590 cm^{-1} in transmittance spectrum of f-biocarbon confirms formation of C=C [42]. Also, peak at 789 cm^{-1} is a characteristic of C-C bending. These peaks confirm the conversion of bamboo waste into graphitic carbon-like structure. Further, spectrum for f-biocarbon shows a significant peak around 3648 cm^{-1} which is because of O-H stretching vibrations which are characteristic of structural OH groups present in GO. Peak at 1683 cm^{-1} is a characteristic of stretching vibration of C=O of carboxyl group [43]. At the same time, peak at 1590 cm^{-1} has disappeared which also confirms maximum oxidation of C=C. The peak at 1073 cm^{-1} represents C-O stretching vibrations of C-O-C [44]. All these are evidences of functionalisation of the bio-carbon with oxygen functional groups. However, in the FTIR spectrum of f-biocarbon-Fe_3O_4, all these peaks are less intense which is due to the anchoring of the Fe_3O_4 nanoparticles over the oxygen functionalities of f-biocarbon, thereby reducing them. Also, addition of the significant peak at 580 cm^{-1}, which represents Fe-O band of Fe_3O_4 confirms formation and attachment of Fe_3O_4 nanoparticles over the f-biocarbon surface [45].

Figure 3 shows XRD pattern of f-biocarbon-Fe_3O_4 nanocomposite particles. Characteristic peaks at 31.42°, 35.28°, 43.24°, 54.42°, 57.42°, and 62.5°, corresponding to planes at (220), (311), (400), (422), (511), and (440), respectively, confirm attachment of Fe_3O_4 nanoparticles on the f-biocarbon particles. These peaks are in accordance with those of inverse cubic spinel phase of Fe_3O_4 nanoparticles [46].

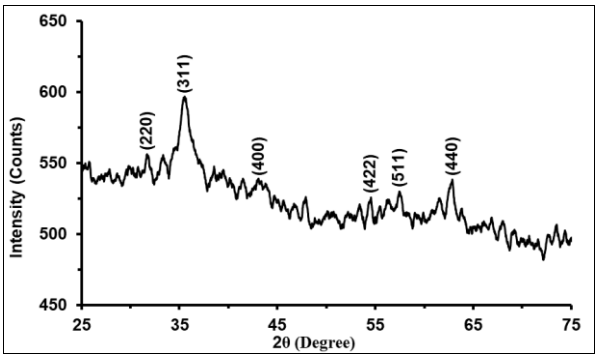

Fig. 3. XRD pattern of f-biocarbon-Fe_3O_4 nanocomposite particles

3.2 Thermal conductivity of f-biocarbon-Fe_3O_4 nanocomposite based nanofluid

Thermal conductivity as a function of temperature of different concentrations of f-biocarbon-Fe_3O_4 nanocomposite based nanofluid is depicted in Figure 4. Thermal conductivity of base fluid water is found to be enhanced by dispersing f-biocarbon-Fe_3O_4 nanocomposite particles into it. The f-biocarbon-Fe_3O_4 nanocomposite particles are composed of metal oxide nanoparticles (Fe_3O_4 nanoparticles) attached to graphite-like carbon support. Attachment of both these components to each other provides a synergistic effect in improving thermal conductivity of nanofluid. Firstly, Fe_3O_4 nanoparticles have high thermal conductivity. Secondly, attachment of Fe_3O_4 nanoparticles to the f-biocarbon particles prevents their agglomeration. The biocarbon, acting as support for the Fe_3O_4 nanoparticles, possesses an increased surface area that provides scope for Fe_3O_4 coverage and further promotes heat transfer. It is clear from the graph that thermal conductivity of the prepared nanofluid increases with rise in temperature. With a rise in temperature from 26.25°C to 44.62°C, thermal conductivity of 0.1 vol.% f-biocarbon-Fe_3O_4 nanocomposite based nanofluid increases from 0.811 W/mK to 1.635 W/mK (almost twice). Higher temperature of the nanofluid leads to micro-movement of the dispersed nanoparticles. This is commonly known as their Brownian motion [47]. The f-biocarbon-Fe_3O_4 nanocomposite particles are therefore in intense motion within the nanofluids at higher temperatures which brings about their collision. Higher temperature also decreases the surface energy of the nanoparticles which help them detach from each other which in turn prevents their agglomeration and settling. Prevention of

agglomeration of nanoparticles further eases their Brownian motion. Higher temperature also leads to lessening of the viscosity of base fluid which further enhances the Brownian motion. This also leads to intensified collision of the f-biocarbon-Fe_3O_4 nanocomposite particles which gives rise to conduction of heat through the chain formed by the colliding nanoparticles [48]. At the same time, this kind of micro-motion of nanoparticles throughout the fluid induces micro-convection currents which further helps in dissipating the heat and enhancing thermal conductivity of fluid.

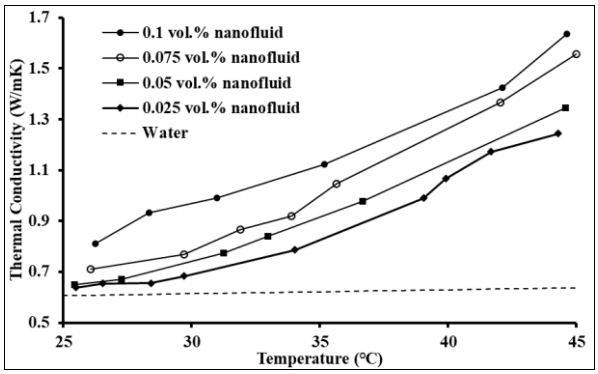

Fig. 4. Thermal conductivity of f-biocarbon-Fe_3O_4 nanocomposite based nanofluids at different concentrations and temperatures

Further, it is also clear from the graph that thermal conductivity of nanofluid is a function of concentration of f-biocarbon-Fe_3O_4 nanocomposite particles in it. The thermal conductivity value of nanofluid having higher concentration is large at the same temperature. The nanofluid shows an increase in thermal conductivity from 1.244 W/mK to 1.635 W/mK as concentration was increased from 0.025 vol.% to 0.1 vol.%. Thus, a 4-fold increase in concentration of the nanofluid leads to 31.43% enhancement in thermal conductivity. Nanoparticles, being solid entities, possess high thermal conductivity compared to liquid base fluid. By virtue of this, they carry significant amount of thermal energy along with them thereby dissipating the heat throughout the fluid. This effect is more pronounced at higher concentration of the nanofluid due to presence of more nanoparticles. At the same time, micro-convection currents induced by the Brownian motion are more pronounced at higher concentration of the nanoparticles. This plays major role in improving the thermal conductivity of nanofluid having higher concentration. Similarly, larger number of nanoparticles form longer chains thereby exhibiting higher thermal conductivity.
Furthermore, the positive effects of ultrasonication are also evident from the higher thermal conductivity results obtained for the nanofluid. This is related to the smaller size of the Fe_3O_4 nanoparticles achieved by the cavitational effects. The smaller-sized nanoparticles have high thermal conductivity due to increased surface area. Similarly, the uniform distribution of the Fe_3O_4 nanoparticles over the f-biocarbon surface, obtained as a result of ultrasound-assisted synthesis, is another factor contributing to the achievement of high thermal conductivity. Prevention of agglomeration of the Fe_3O_4 nanoparticles due to this has further resulted in prevention of overlapping of their surface area thereby allowing maximum surface area to take part in heat conduction.

3.3 Empirical model for thermal conductivity of f-biocarbon-Fe_3O_4 nanocomposite based nanofluid

Data acquired for thermal conductivity of f-biocarbon-Fe_3O_4 nanocomposite based nanofluid was used to determine an empirical model by the use of polynomial regression. The obtained Equation (1) relates thermal conductivity of nanofluid (k) in W/mK to its volume fraction (φ) and temperature (T) in °C.

$$k = 343.707\varphi + 0.0392T - 0.57039 \quad (1)$$

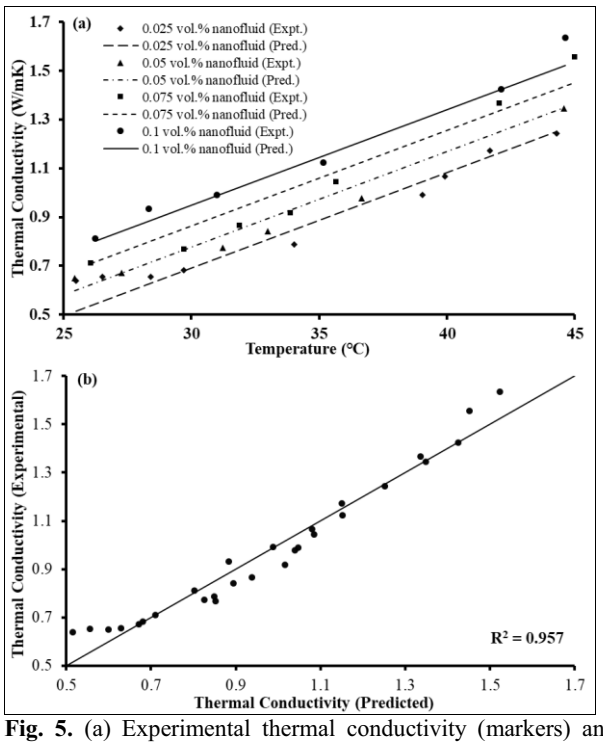

Fig. 5. (a) Experimental thermal conductivity (markers) and predicted values (lines) and (b) scatter plot for predicted thermal conductivity of f-biocarbon-Fe_3O_4 nanocomposite based nanofluids

Figure 5(a) shows experimental and predicted thermal conductivity of f-biocarbon-Fe_3O_4 nanocomposite based nanofluid. Predicted thermal conductivity is much closer to the experimental thermal conductivity. The scatter plot shown in Figure 5(b) for predicted thermal conductivity also confirms accuracy of the model exhibiting R^2 value of 0.957. Thus, proposed empirical model can well predict thermal conductivity of f-biocarbon-Fe_3O_4 nanocomposite based nanofluid.

4 Conclusions

Synthesis of f-biocarbon-Fe_3O_4 nanocomposite particles was accomplished by attaching Fe_3O_4 nanoparticles over

functionalized bio-based graphitic carbon using the ultrasound-assisted coprecipitation method. Thermal conductivity of water-based nanofluid prepared using the synthesized nanocomposite particles was then examined. Such an investigation on bio-based nanofluid for thermal energy transport has been conducted for the first time. For this, the bio-based graphitic carbon (biocarbon) derived from bamboo waste was functionalized with oxygen functionalities to synthesize functionalized biocarbon (f-biocarbon). Attachment of Fe_3O_4 nanoparticles over the f-biocarbon particles was confirm by SEM, FTIR, and XRD analysis. Further, water-based nanofluids prepared using the synthesized nanoparticles showed greater thermal conductivity compared to water. Thermal conductivity of nanofluid increased with rise in concentration and temperature. The main reason for this was the increased Brownian motion of f-biocarbon-Fe_3O_4 nanocomposite particles and their constant collision which increased chances of heat conduction through them. Furthermore, the cavitational effect of ultrasound during nanocomposite synthesis has also proved to be very important. A new correlation relating thermal conductivity with concentration and temperature of f-biocarbon-Fe_3O_4 nanocomposite based nanofluid has also been proposed which satisfactorily predicts the experimental data exhibiting an R^2 value of 0.957.

Authors are thankful to Laxminarayan Institute of Technology for support and encouragement.

References

1. B.A. Bhanvase, D.P. Barai, S.H. Sonawane, N. Kumar, S.S. Sonawane, *Intensified Heat Transfer Rate With the Use of Nanofluids*, in Handbook of Nanomaterials for Industrial Applications, Elsevier, 2018: pp. 739–750
2. D.P. Barai, K.K. Chichghare, S.S. Chawhan, B.A. Bhanvase, *Synthesis and Characterization of Nanofluids: Thermal Conductivity, Electrical Conductivity and Particle Size Distribution*, in Nanotechnology for Energy and Environmental Engineering, Springer, 2020: pp. 1–49
3. K.K. Chichghare, D.P. Barai, B.A. Bhanvase, *Applications of Nanofluids in Solar Thermal Systems*, in Nanofluids and Their Engineering Applications, CRC Press, 2019: pp. 275–314
4. R.N. Radkar, B.A. Bhanvase, D.P. Barai, S.H. Sonawane, Mater. Sci. Energy Technol. **2**, 161–170 (2019)
5. T.K. Hong, H.S. Yang, C.J. Choi, J. Appl. Phys. **97**, 064311 (2005)
6. B.A. Bhanvase, M.R. Sarode, L.A. Putterwar, A. K.A., M.P. Deosarkar, S.H. Sonawane, Chem. Eng. Process. Process Intensif. **82**, 123–131 (2014)
7. K.S. Hwang, S.P. Jang, S.U.S. Choi, Int. J. Heat Mass Transf. **52**, 193–199 (2009)
8. K. Ahmad, C. Wan, M.A. Al-Eshaikh, A.N. Kadachi, Appl. Surf. Sci. **474**, 2–8 (2019)
9. A. Godymchuk, I. Papina, E. Karepina, D. Kuznetsov, I. Lapin, V. Svetlichnyi, J. Nanoparticle Res. **21**, (2019)
10. E.A. Campos, D.V.B. Stockler Pinto, J.I.S. de Oliveira, E.D.C. Mattos, R.D.C.L. Dutra, J. Aerosp. Technol. Manag. **7**, 267–276 (2015)
11. Y. Wang, Z. Shi, Y. Huang, Y. Ma, C. Wang, M. Chen, Y. Chen, J. Phys. Chem. C. **113**, 13103–13107 (2009)
12. M.F. El-Kady, Y. Shao, R.B. Kaner, Nat. Rev. Mater. **1**, 1–14 (2016)
13. J. Liu, Y. Xue, M. Zhang, L. Dai, MRS Bull. **37**, 1265–1272 (2012)
14. G. Centi, S. Perathoner, ChemSusChem. **4**, 913–925 (2011)
15. C. Wang, M. Waje, X. Wang, J.M. Tang, R.C. Haddon, Y. Yan, Nano Lett. **4**, 345–348 (2004)
16. N.A.C. Sidik, M.N.A.W.M. Yazid, S. Samion, Int. J. Heat Mass Transf. **111**, 782–794 (2017)
17. D.P. Barai, B.A. Bhanvase, S.H. Sonawane, Ind. Eng. Chem. Res. **59**, 10231–10277 (2020)
18. A. Arshad, M. Jabbal, Y. Yan, D. Reay, J. Mol. Liq. **279**, 444–484 (2019)
19. S. Koçak Soylu, İ. Atmaca, M. Asiltürk, A. Doğan, Appl. Therm. Eng. **157**, 113743 (2019)
20. A. Ceylan, K. Jastrzembski, S.I. Shah, Metall. Mater. Trans. A Phys. Metall. Mater. Sci. **37**, 2033–2038 (2006)
21. A. Lanjewar, B. Bhanvase, D. Barai, S. Chawhan, S. Sonawane, Period. Polytech. Chem. Eng. **64**, 271-282 (2019)
22. B.A. Bhanvase, S.D. Kamath, U.P. Patil, H.A. Patil, A.B. Pandit, S.H. Sonawane, Chem. Eng. Process. Process Intensif. **104**, 172–180 (2016)
23. N.R. Koshta, B.A. Bhanvase, S.S. Chawhan, D.P. Barai, S.H. Sonawane, Indian Chem. Eng. **62**, 202-215 (2020)
24. S.S. Chawhan, D.P. Barai, B.A. Bhanvase, Mater. Today Commun. **23**, 101148 (2020)
25. H.A. Sarode, D.P. Barai, B.A. Bhanvase, R.P. Ugwekar, V. Saharan, Mater. Chem. Phys. **251**, 123102 (2020)
26. H. Mandhare, D. P. Barai, B. A. Bhanvase, V.K.V.K. Saharan, Mater. Res. Innov. **24**, 433–441 (2020)
27. D.P. Barai, B.A. Bhanvase, V.K. Saharan, Ind. Eng. Chem. Res. **58**, 8349–8369 (2019)
28. K. Singh, D.P. Barai, S.S. Chawhan, B.A. Bhanvase, V. Saharan, Mater. Today Commun. **26**, 101986 (2021)
29. M.A. Yahya, Z. Al-Qodah, C.W.Z. Ngah, Renew. Sustain. Energy Rev. **46**, 218–235 (2015)
30. C.R. Correa, A. Kruse, Materials (Basel). **11**, 1568 (2018)
31. Z. Wang, S. Yun, X. Wang, C. Wang, Y. Si, Y. Zhang, H. Xu, Ceram. Int. **45**, 4208–4218 (2019)

32. J. Zhang, H. Chen, Z. Ma, H. Li, Y. Dong, H. Yang, L. Yang, L. Bai, D. Wei, W. Wang, J. Alloys Compd. **832**, 155029 (2020)
33. A. Pistone, C. Espro, Curr. Opin. Green Sustain. Chem. **26**, 100374 (2020)
34. V. Siipola, S. Pflugmacher, H. Romar, L. Wendling, P. Koukkari, Appl. Sci. **10**, 788 (2020)
35. A. Kumar, V. Goyal, N. Sarki, B. Singh, A. Ray, T. Bhaskar, A. Bordoloi, A. Narani, K. Natte, ACS Sustain. Chem. Eng. **8**, 15740–15754 (2020)
36. P. Esmaeilzadeh, Z. Fakhroueian, A.A.M. Beigi, J. Nano Res. **16**, 89–96 (2011)
37. N. Abraham, A. Rufus, C. Unni, D. Philip, J. Mater. Sci. Mater. Electron. **28**, 16527–16539 (2017)
38. E.C. Okonkwo, E.A. Essien, E. Akhayere, M. Abid, D. Kavaz, T.A.H. Ratlamwala, Sol. Energy. **170**, 658–670 (2018)
39. R. Sadri, M. Hosseini, S.N. Kazi, S. Bagheri, A.H. Abdelrazek, G. Ahmadi, N. Zubir, R. Ahmad, N.I.Z. Abidin, J. Colloid Interface Sci. **509**, 140–152 (2018)
40. G. Adewumi, F. Inambao, Int. J. Renew. Energy Res. **10**, 1302–1306 (2020)
41. W.S. Hummers, R.E. Offeman, J. Am. Chem. Soc. **80**, 1339 (1958)
42. C. Galande, A.D. Mohite, A. V. Naumov, W. Gao, L. Ci, A. Ajayan, H. Gao, A. Srivastava, R.B. Weisman, P.M. Ajayan, Sci. Rep. **1**, 85 (2011)
43. L. Shahriary, A.A. Athawale, Int. J. Renew. Energy Environ. Eng. **2**, 58–63 (2014)
44. T.F. Emiru, D.W. Ayele, Egypt. J. Basic Appl. Sci. **4**, 74–79 (2017)
45. T. Togashi, T. Naka, S. Asahina, K. Sato, S. Takami, T. Adschiri, Dalt. Trans. **40**, 1073–1078 (2011)
46. M.C. Morris, H.F. McMurdie, E.H. Evans, B. Paretzkin, J.H. de Groot, C.R. Hubbard, S.J. Carmel, Standard X-ray Diffraction Powder Patterns, U.S. Government Printing Office, Washington D.C., 1976
47. C.C. Li, N.Y. Hau, Y. Wang, A.K. Soh, S.P. Feng, Phys. Chem. Chem. Phys. **18**, 15363–15368 (2016)
48. X. Wang, X. Xu, S.U.S. Choi, S.U. S. Choi, X. Wang, X. Xu, S.U. S. Choi, J. Thermophys. Heat Transf. **13**, 474–480 (1999)